ACS APPLIED MATERIALS & INTERFACES

Research Article

www.acsami.org

Highly Moldable Electrospun Clay-Like Fluffy Nanofibers for Three-Dimensional Scaffolds

Slgirim Lee,[†,§] Sunghwan Cho,[‡,§] Minhee Kim,[†] Gyuhyung Jin,[†] Unyong Jeong,*[,‡] and Jae-Hyung Jang*[,†]

[†]Department of Chemical and Biomolecular Engineering, Yonsei University, 134 Shinchon-dong, Seoul, Korea

[‡]Department of Materials Science and Engineering, Yonsei University, 134 Shinchon-dong, Seoul, Korea

Supporting Information

ABSTRACT: The development of three-dimensional polymeric systems capable of mimicking the extracellular matrix is critical for advancing tissue engineering. To achieve these objectives, three-dimensional fibrous scaffolds with "clay"-like properties were successfully developed by coaxially electrospinning polystyrene (PS) and poly(ε-caprolactone) (PCL) and selective leaching. As PS is known to be nonbiodegradable and vulnerable to mechanical stress, PS layers present at the outer surface were removed using a "selective leaching" process. The fibrous PCL scaffolds that remained after the leaching step exhibited highly advantageous characteristics as a tissue engineering scaffold, including moldability (i.e., clay-like), flexibility, and three-dimensional structure (i.e., cotton-like). More so, the "clay-like" PCL fibrous scaffolds could be shaped into any desired form, and the microenvironment within the clay scaffolds was highly favorable for cell expansion both in vitro and in vivo. These "electrospun-clay" scaffolds overcome the current limitations of conventional electrospun, sheet-like scaffolds, which are structurally inflexible. Therefore, this work extends the scope of electrospun fibrous scaffolds toward a variety of tissue engineering applications.

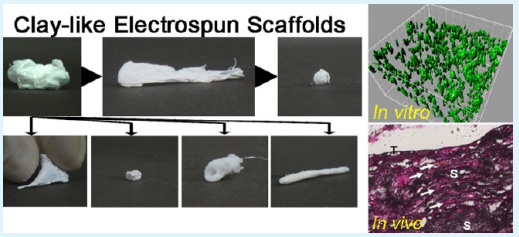

KEYWORDS: *clay scaffold, 3D scaffold, tissue engineering, electrospinning, cellular infiltration, selective leaching*

1. INTRODUCTION

Modulating the ambient microenvironment of target cellular structures can play a pivotal role in triggering tissue morphogenesis in living systems. Therefore, tissue engineering approaches often require the presentation of structural cues that precisely mimic the extracellular matrix (ECM) to control the structure of the resulting tissue and enable the induction of key cellular processes such as differentiation, proliferation, and migration. Various types of tissue engineering scaffolds have been modified to mimic the ECM microenvironment using a variety of methods, including gas foaming/particulate leaching,[1,2] phase separation,[3] hydrogelation,[4] or the formation of self-assembled macromolecules.[5] However, these efforts still suffer from inherent challenges associated with the development of tissue engineering scaffolds, such as porosity, structural flexibility, mechanical integrity, cellular infiltration, and an inability to mimic natural ECM fully.[6]

Fibrous scaffolds constructed by electrospinning have emerged as powerful tools to solve the challenges discussed above due to their structural similarity to the natural ECM, thus making them a suitable material to guide new tissue formation. In addition to their similarity to ECM, electrospun scaffolds have many advantageous properties including amenability to a wide range of materials such as synthetic polymers,[7] proteins,[8] metals,[9] and ceramics,[10] large surface/volume ratios,[11] and an ability to guide cellular patterns.[12] For these reasons, electrospun fibrous scaffolds have recently been employed as physical cues in a variety of tissue engineering applications, such as the regeneration of vascular structures,[13] bones,[14] and peripheral or central nervous systems.[15,16] Despite their advantages, these scaffolds have not yet been extensively applied in tissue engineering due to limitations including their inefficiency in generating three-dimensional structures with various volumetric shapes due to their structural inflexibility, preventing the preparation of diverse shapes. Electrospinning typically results in a sheet-like, thin layer that does not allow for cellular infiltration across the scaffold interior.[17] This structural limitation is caused by the dense accumulation of nanofibers one after another in a neat pile. Therefore, the discovery of novel design parameters that can introduce structural versatility to the electrospun scaffolds will significantly advance tissue engineering technology.

This structural challenge of electrospinning has been addressed using multiple approaches including multilayering processes,[13] self-assembly processes,[18] collector modifications,[19,20] coaxial electrospinning,[21] porogen addition,[22] and performing electrospinning under wet conditions.[14] Additionally, bundling fibers prepared from aligned two-dimensional mats,[23] collecting nanofibers using a bowl with metallic needles,[24] and stacking biocompatible proteins with polyethylene glycol fibers on a conductive flat substrate[25] were employed to modulate three-dimensional structures of electrospun fibers. All of these unique methodologies have been effective in forming three-dimensional, electrospun fibrous

Received: October 20, 2013
Accepted: December 25, 2013
Published: December 25, 2013

   dx.doi.org/10.1021/am404627r | ACS Appl. Mater. Interfaces 2014, 6, 1082−1091

scaffolds, but these tools still lack the structural flexibility to freely form various shapes, which may be indispensable to enable use in a variety of tissue engineering applications. Importantly, the majority of these currently available approaches requires the manipulation of the apparatus or the collector, which can be laborious or costly.

The current study demonstrates a novel platform to fabricate fluffy, highly moldable "electrospun-clay" scaffolds. Recently, Xu et al. developed a novel method to fabricate fluffy nanofibers by simply electrospinning polystyrene.[26] The repulsion between the electrospun nanofibers caused by the accumulation of negative charges, which is inducted under the influence of a strong electric field, is believed to cause the fluffy structure. The exact mechanism requires a thorough investigation for expanding the available polymer species to biodegradable polymers. The current study takes advantage of this "fluffy" property of electrospun polystyrene fibers. Coaxial electrospinning (Figure 1A) was used to generate fibrous scaffolds with core−shell structures, with poly(ε-caprolactone) (PCL) designed to reside in the inner core and polystyrene (PS) in the outer layer (PCL/PS). The exterior PS layers played a key role as a building block to formulate three-dimensional fluffy structures. After the fluffy scaffolds with the core−shell structure were produced, the polystyrene in the shell layer was selectively leached out due to its lack of biodegradability and mechanical strength as a tissue engineering scaffold,[27,28] resulting in three-dimensional fibrous PCL scaffolds. Importantly, the resulting PCL fibers with cotton-like shapes could be highly elongated and molded into arbitrary three-dimensional shapes without the need for an additional sophisticated apparatus, similar to commercial rubber clay. The nanofiber scaffolds were characterized using in vitro and in vivo models to illustrate the potential of this "electrospun clay" for use in numerous tissue engineering applications. Furthermore, adeno-associated viral vectors (AAVs) were immobilized onto the fibers to examine the possibility of applying these PCL−clay fibrous scaffolds in an inductive tissue engineering approach. The facile methodology to fabricate the "electrospun clay" scaffolds developed in this study can overcome the current limitations of fibrous scaffolds resulting from their structural inflexibility, thereby extending the applications of electrospun scaffolds for tissue engineering.

2. EXPERIMENTAL SECTION

2.1. Materials. Polystyrene (PS, M_n = 170 000 g/mol), poly(ε-caprolactone) (PCL, M_n = 80 000 g/mol), hematoxylin, and eosin were purchased from Sigma-Aldrich (St. Louis, MO). Tetrahydrofuran (THF; Daejung, Seoul, Korea) and dimethylformamide (DMF; Duksan, Seoul, Korea) were used as solvents to dissolve PS and PCL chains.

2.2. Coaxial Electrospinning of PCL/PS Core−Sheath Mats. Prior to producing "electrospun-clay" fibrous scaffolds, three-dimensional fluffy PS−PCL composite scaffolds were fabricated using a coaxial electrospinning system (ESR 100, NanoNC, Seoul, Korea). Polymers for the core and shell solutions were dissolved separately in a mixture of THF and DMF (THF:DMF = 1:1, v:v). PS and PCL were dissolved in the solvent at 15% and 15% (w/v), respectively, and each solution was separately charged in a different syringe prior to producing the shell layer (PS) and the core layer (PCL). Figure 1A presents a detailed illustration of the fabrication protocol. Each solution was fed to the homemade nozzle, which is composed of an inner (30G, inner diameter = 160 μm) and an outer needle (22G, inner diameter = 410 μm), and subsequently electrospun onto the grounded aluminum foil collector at the various feed rates shown in Table 1. A high-voltage DC power supply was used to apply voltage

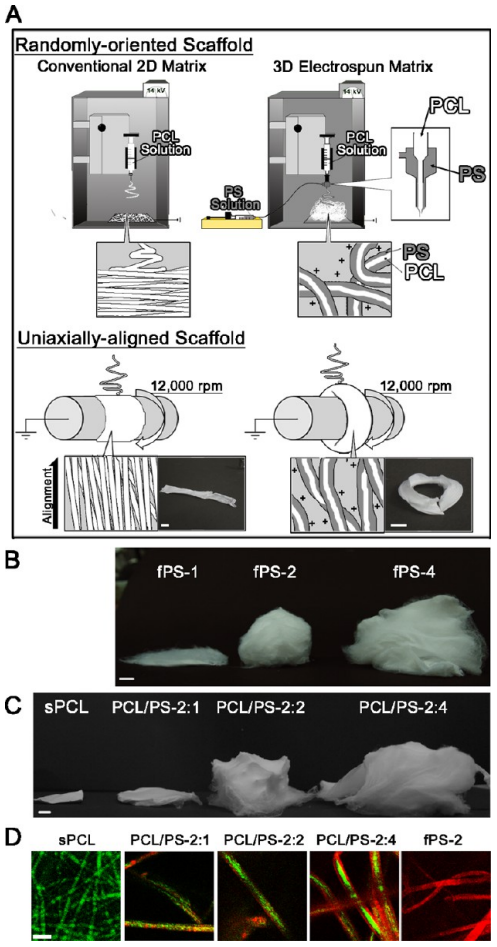

Figure 1. Fabrication of fluffy PCL/PS composite fibrous scaffolds. (A) Schematic illustration depicting (i) the conventional system used to form sheet-like PCL scaffolds (top-left) and uniaxially aligned scaffolds (bottom-left) and (ii) the coaxial electrospinning system used to form fluffy PCL/PS composite scaffolds (top-right) and uniaxially aligned, fluffy PCL/PS composite scaffolds (bottom-right). (B) Digital photographs of fluffy electrospun PS scaffolds (fPS) and (C) fluffy electrospun PCL/PS composite scaffolds before leaching. The scale bars in (B) and (C) represent 1 cm. (D) Confocal laser scanning microscopic images demonstrating the interfaces of core (coumarin)−shell (rhodamine) structures as a function of PS feed rate. The scale bar represents 5 μm.

Table 1. Experimental Conditions Used to Prepare Fluffy Nanofiber Mats and the Abbreviations Designating Each Scaffold Formulation

	shell solution (PS) (mL h^{-1})	core solution (PCL) (mL h^{-1})	abbreviation
PS Only	1	0	fPS-1
	2	0	fPS-2
	4	0	fPS-4
PCL Only	0	2	sPCL
Before Leaching	1	2	PCL/PS-2:1
	2	2	PCL/PS-2:2
	4	2	PCL/PS-2:4
After Leaching	1	2	fPCL-2:1
	2	2	fPCL-2:2
	4	2	fPCL-2:4
Materials	PS (M_n = 170 kDa)	PCL (M_n = 80 kDa)	
Solvent	THF:DMF = 1:1		

dx.doi.org/10.1021/am404627r | ACS Appl. Mater. Interfaces 2014, 6, 1082−1091

(14 kV) between the spinneret and the collector, which was set at a distance of 13 cm. As control conditions, either a PS (15% w/v) or PCL solution (15% w/v) was fed into the 18G stainless spinneret and electrospun at a rate of 2 mL/h to form fluffy PS scaffolds (fPS) or sheet-type fibrous PCL scaffolds (sPCL), respectively. To confirm the core−shell structures of the fibers, each polymer solution (PCL and PS) was mixed with coumarin (Sigma-Aldrich) and rhodamine B (Sigma-Aldrich) prior to fiber production. Subsequently, the structures of the core−shell fibers containing the fluorescent dyes were observed under the confocal laser scanning microscope at the Yonsei Center for Research Facilities (LSM510META, Carl Zeiss, Thornwood, NY, USA).

2.3. Fabrication of "PCL−Clay" Fibrous Scaffolds. The electrospun PS−PCL composite scaffolds with a core−shell structure were collected and dried for at least 6 h at room temperature. Subsequently, the scaffolds were vigorously agitated in prechilled DMF for 5 min to selectively leach out the outer PS layer. The immersed scaffolds were transferred to a container with fresh DMF and vigorously washed to remove the residual PS. This selective leaching procedure was repeated five times. Subsequently, the scaffolds were rinsed three times with ethanol and distilled water, lyophilized overnight, and kept in a desiccator until use. To alter the morphologies of the electrospun-clay scaffolds to the desired shapes, the scaffolds obtained after the selective leaching step were molded into a homemade cylindrical frame, rolled using a thin wire, and manually forged to form a human nose. Additionally, uniaxially aligned PCL−clay matrices were also successfully fabricated using the same apparatus with an additional rotating mandrel (1200 rpm).

2.4. Characterization of the Physical and Chemical Properties of Electrospun PCL−Clay Scaffolds. The physical and chemical properties of PCL−clay electrospun fibrous scaffolds were characterized in terms of fiber morphologies, mechanical strength, and chemical composition. The morphologies of the nanofibrous structures were investigated using field emission scanning electron microscopy (FE-SEM) (JEOL-7001F, JEOL, Japan) at an accelerating voltage of 15 kV. To test the mechanical properties, the tensile strengths of the scaffolds were characterized in the axial direction with a universal testing machine (Multi Test 1-i, Mecmesin, Slinfold, UK) under a 50 N power cell. The presence of residual PS components after the "selective" leaching step with DMF was analyzed by Fourier transform infrared (FT-IR) spectroscopy (Spectrum 100, Perkin-Elmer, Waltham, MA, USA). The solubility of PCL and PS in DMF at different temperatures was determined by measuring thickness variations of PCL and PS films, which were soaked in DMF for 1 h. Each film was fabricated on Si wafers at 2500 rpm for 30 s using a spin-coater (Spin-1200D, Midas, Daejeon, Korea). Subsequently, each film was immersed in DMF prechilled at different temperatures (−20, −10, 0, 10, and 20 °C) for 1 h and spun at 2500 rpm for 30 s to remove the residue of DMF. The thickness of each dried film was measured using ellipsometry (SE MG-Vis 1000, Nanoview, Ansan, Korea). Finally, to quantify the porosity of the clay-like PCL scaffolds, the specific pore volume, which is defined as the volume of pores per unit mass of scaffolds, was measured using the following equation[25]

$$V_{sp} = \frac{V_{pore}}{m_{scaffold}} = \frac{V_{scaffold}}{m_{scaffold}} - \frac{1}{\rho_{material}}$$

where V_{sp} is the specific pore volume; V_{pore} is the volume of pores in the scaffolds; $m_{scaffold}$ is the mass of scaffolds; $V_{scaffold}$ is the volume of the scaffolds; and $\rho_{material}$ is the density of PCL (1.145 g/cm^3). Two-dimensional scaffolds (i.e., sPCL, fPCL-2:1) were cut into 1 cm × 1.5 cm pieces, and fluffy scaffolds (i.e., fPCL-2:2 and fPCL-2:4) were prepared into rectangular shapes. Finally, the volume and mass of each scaffold were measured to calculate the specific pore volume.

2.5. Cell Culture. Cellular infiltration into the scaffolds was studied using NIH3T3 cells derived from mouse fibroblasts, and AAV293 cells (Stratagene, La Jolla, CA, USA) were utilized for packaging adeno-associated viral (AAV) vectors. These cell lines were cultured in Dulbecco's modified Eagle's medium (DMEM; Invitrogen, Carlsbad, CA, USA) with 10% fetal bovine serum (FBS) (Invitrogen) and 1% penicillin and streptomycin (Invitrogen) at 37 °C and 5% CO_2. The HEK293T cell line was also used as an in vitro model system to demonstrate cellular transduction by AAV vectors immobilized onto the PCL−clay fibers, thus illustrating the potential of the scaffolds as a platform to deliver soluble factors.

2.6. AAV Packaging. In this study, AAV r3.45, a specialized vector newly engineered using directed evolution to infect a cell type nonpermissive to wild type AAV2,[29] was used as a gene delivery vehicle to transduce HEK293T cells adhered onto the electrospun fibers. Prior to adsorption onto the fibers, recombinant AAV r3.45 vectors carrying cDNA coding for green fluorescent protein (GFP) or luciferase driven by a cytomegalovirus (CMV) promoter were packaged by transient transfection.[30] An equal mass (17 μg) of three plasmids, including a CMV GFP or luciferase vector plasmid containing the inverted terminal repeat (ITF) (pAAV CMV GFP or pAAV CMV luc), an AAV helper plasmid (carrying cap r3.45), and an adenoviral helper plasmid (Stratagene), was transfected into AAV 293 cells using calcium phosphate as previously described.[30] Subsequently, the resulting viral vectors were harvested and purified using a 1 mL HiTrap heparin column (GE Healthcare, Pittsburgh, PA, USA) according to the manufacturer's instructions. Finally, DNase-resistant genomic titers were determined by quantitative PCR (qPCR) (Mini Opticon, Bio-Rad, Hercules, CA, USA).

2.7. In Vitro Characterization of PCL−Clay Scaffolds. To investigate the cellular infiltration across the scaffolds fabricated by the PCL−clay fibers, NIH3T3 cells (5×10^4 cells in 5 μL) were embedded into scaffolds (cylindrical fPCL-2:2 scaffolds: 5 mm diameter × 1 mm height; and sPCL scaffolds: 5 mm width × 5 mm length) attached to a 96-well tissue culture plate, and the cellular distributions within the scaffolds were visualized by staining the cells using either hematoxylin/eosin (H/E; Sigma-Aldrich) or fluorescein diacetate (FDA; Sigma-Aldrich). Prior to cell culture, scaffolds were immersed in 70% ethanol for 30 min for sterilization and vigorously rinsed three times with PBS. For H/E staining, scaffolds were rinsed twice with PBS after 4 days of culture, and the cells within the scaffolds were fixed overnight with prechilled 4% phosphate-buffered paraformaldehyde (PFA; Sigma-Aldrich) at 4 °C and frozen in the Optimal Cutting Temperature compound (OCT, Sakura Finetek USA Inc., Torrance, CA, USA). Subsequently, sections were cut (16 μm) using a cryostat microtome (Leica CM1850, Leica Biosystems, Germany) and stained with H/E as previously described.[31] Furthermore, live cells cultured within the PCL−clay scaffolds for 4 days were stained with FDA (15 μg/mL) dissolved in PBS and observed under the confocal laser scanning microscope at the Yonsei Center for Research Facilities (LSM510META, Carl Zeiss, Thornwood, NY, USA). The morphologies of the FDA-labeled NIH3T3 cells adherent to the fibers were reconstructed three-dimensionally using Imaris 7.4.2. (Bitplane, UK). Additionally, the cellular viabilities of NIH3T3 cells or HEK293T cells cultured within the scaffolds were evaluated using a WST-1 assay kit (Roche Applied Science, Indianapolis, IN, USA) according to the manufacturer's protocol. At 2 and 7 days postculture, the colorimetric changes of the supernatants containing scaffolds were measured at 440 nm using a spectrophotometer (Nanodrop 2000, Thermo Scientific, West Palm Beach, FL, USA). Finally, to investigate the gene delivery capabilities of the resulting scaffolds, HEK293T cells, which are highly permissive to AAV vectors, were embedded into the scaffolds containing viral vectors. AAV vectors encoding GFP or luciferase were used to visualize cellular transduction or quantify gene expression within the scaffolds, respectively. AAV r3.45 vectors were used to maximize cellular transduction compared to wild-type AAV2, as previously demonstrated.[29] To immobilize the viral vectors onto the fibers, the scaffolds were soaked into 1.0×10^9 viral genomes in 100 μL and incubated at 37 °C overnight. HEK293T cells (10^5 cells in 3 μL) were subsequently seeded into the scaffolds and cultured for 4 days prior to analysis. The fluorescence images of GFP-expressing cells were observed under a confocal laser scanning microscope, and the luciferase gene expression was measured on a luminometer (LB96P, EG & G, Berthold, Germany) using the luciferase assay system (Promega, Madison, WI, USA), with levels normalized to the initial cell seeding numbers.

2.8. In Vivo Cellular Infiltration. To investigate both the cellular infiltration toward the inner space of the scaffolds formed using the PCL−clay fibers and the integrity of the scaffolds upon implantation, both randomly oriented and uniaxially aligned PCL−clay scaffolds were implanted subcutaneously into female C57BL/6 mice (20−22 g). The conditions examined in this study include (i) cylindrical, three-dimensional scaffolds (5 mm diameter × 1 mm height) molded using the fPCL-2:2 fibers; (ii) conventional, randomly oriented sheet-type PCL scaffolds (sPCL; rectangular shape, 5 mm width × 5 mm length); (iii) uniaxially aligned scaffolds formed by fPCL-2:2 fibers; and (iv) uniaxially aligned, sheet-type PCL scaffolds (n = 10 for all conditions). Scaffolds with adjacent tissues were retrieved at 7 days and 20 days postimplantation, fixed in 4% PFA overnight at 4 °C, and subsequently immersed in 10% and 30% sucrose solution. Tissue blocks were frozen in OCT, and sections were cut (16 μm) using a cryostat microtome and stained with H&E to examine both the cellular internalization within the implanted scaffolds and the scaffold integrity against cellular contractile forces upon implantation. All the experimental procedures followed guidelines for the care and handling of laboratory animals and were approved by the Yonsei Laboratory Animal Research Center Institutional Animal Care and Use Committee (YLARC-IACUC, Yonsei University, Korea).

2.9. Statistical Analysis. All statistical analyses were performed using a one-way analysis of variance (ANOVA) with a post hoc Dunnett's test using the SPSS 18.0 software package (IBM Corporation, Somers, NY, USA). P values <0.05 were considered to be statistically significant.

3. RESULTS AND DISCUSSION

The procedure utilized to obtain the fluffy PCL nanofibers involves the production of PCL/PS fluffy nanofibers followed by selective removal of the PS sheath. As shown in Figure 1A, the apparatus used to form the fluffy core−shell structures was basically identical to conventional coaxial electrospinning tools, demonstrating the ease and accessibility of this protocol. In addition, uniaxially aligned PCL/PS electrospun nanofibers were also successfully fabricated by the same apparatus with an additional rotating mandrel (1200 rpm) (Figure 1A). Because the formation of the core−sheath fluffy nanofibers was governed by the PS, the appropriate experimental conditions for obtaining fluffy PS nanofibers were examined first. Following the literature,[26] PS (M_n = 170 000) was dissolved in a mixture solvent (tetrahydrofuran (THF):dimethylformamide (DMF) = 1:1, v/v) to adjust the evaporation rate and polarity of the solution. The concentration of the PS solution was fixed at 15 wt % in this study. As described in Table 1, additional parameters such as feed rates (i.e., the feed rates of the shell and core layers) and the tip-to-collector distance were systematically optimized to form self-assembled, three-dimensional fluffy structures. The formation of the PS fluffy structure was initially optimized, which was sensitive to the feed rate of the PS solution (Figure 1B). The PS mat was slightly fluffy at a feed rate of 1 mL h^{-1} (fPS-1), whereas fluffy mats were routinely obtained at 2 mL h^{-1} (fPS-2). A cotton-like structure was prominent when the feed rate was larger than 4 mL h^{-1} (fPS-4). This dependence on feed rates is attributed to the increased amount of remnant solvent in the as-spun nanofibers as the feed rate increased (Figure S1, Supporting Information). It was reported that the rapid transfer of negative charges on the spun fibers to the collector electrode is the crucial factor for 3D stacking of nanofibers.[25] The solvent (DMF) used in this study has a higher dipole moment than PS or PCL. The solvent on the surface area of the fibers is expected to reduce the surface resistivity of the fibers, hence the negative charges can be transferred to the collector more effectively than dry fibers.[25]

In parallel with the core−sheath approach, the production of fluffy composite nanofiber mats was attempted with a mixture solution of PS and PCL using a single nozzle (32G). PCL (M_n = 80 000) was dissolved in the same mixture solvent (THF:DMF = 1:1, v/v) at a concentration of 15 wt % and blended with PS solution at ratios of 2:1, 2:2, and 2:4 (PCL solution:PS solution, v/v). The mixed solutions were electrospun from a single nozzle to a flat aluminum collector. Although fluffy structures were obtained from the blended solution (Figure S2, Supporting Information), selective dissolution of the PS phase from the fluffy PCL−PS blended-composite nanofibers resulted in disconnection of the resulting PCL nanofibers, causing the fluffy structure to collapse (data not shown).

The fluffy structure was maintained after dissolving PS from the composite nanofibers by using PCL/PS core−sheath nanofibers obtained by coaxial electrospinning. A PCL solution and a PS solution were injected through the inner and outer nozzle, respectively (Figure 1A). The electrospinning conditions were slightly modified from those employed for producing the PS fluffy nanofibers. Figure 1C exhibits the core−sheath nanofiber mats obtained at different polymer solution feed rates. To compare the structure of the resulting nanofiber mats with that of the PS nanofiber mat, the feed rate of the PCL solution was fixed at 2 mL h^{-1}, and the feed rate of the PS solution was maintained at the same rate used for the pure PS nanofibers (1, 2, and 4 mL h^{-1}). The numbers (i.e., 1, 2, and 4) in the abbreviations of the scaffold formulations indicate the feed rates of the corresponding polymer solutions; for example, PCL/PS-2:4 represents the scaffold formed with a PCL feed rate of 2 mL h^{-1} and a PS feed rate of 4 mL h^{-1}. The overall morphologies and dimensions of the core−sheath nanofiber mats were similar to those of the fluffy PS nanofiber mats. No remarkable changes in structure were observed when the PS feed rate was higher than 4 mL h^{-1} (Figure S3, Supporting Information). The PS sheath layer played a key role in the formulation of the fluffy nanofiber mats. The use of a smaller fraction of PS (i.e., PCL/PS-2:1) resulted in typical sheet-type fiber mats, presumably due to the insufficient charge repulsion between the nanofibers (Figure 1C). Figure 1D displays confocal microscopy images of the nanofibers: sPCL, PCL/PS-2:1, PCL/PS-2:2, PCL/PS-2:4, and fPS-2. The PCL/PS-2:4 nanofibers showed a clear core−sheath structure. In the PCL/PS-2:2 nanofibers, the core−sheath structure was predominant, but some nanofibers did not have a clear sheath layer. The PCL/PS-2:1 nanofibers showed a mixed phase because the volume fraction of PS was not sufficient to cover the entire surface of the nanofibers. Additionally, when the feed rate of the shell solution is not high enough to cover the viscoelastic core solution, the "die-swell" effect of the core solution can occur, possibly leading to core−shell reversal or interference from core−shell interfaces.[32]

The PS layer in the PCL/PS core−sheath fluffy nanofibers was selectively leached to obtain PCL nanofibers with a fluffy structure, as PS is not widely used in tissue engineering due to its nonbiodegradability[28] and weak mechanical properties. A detailed schematic illustration of the process of leaching the PS shell layer is presented in Figure 2A. The entire process of producing the three-dimensional PCL fibrous scaffolds could be completed within 30 min (10 min electrospinning and 20 min leaching), significantly less processing time compared with conventional electrospinning techniques. Briefly, PS layers were selectively leached away at −20 °C by immersing the scaffolds

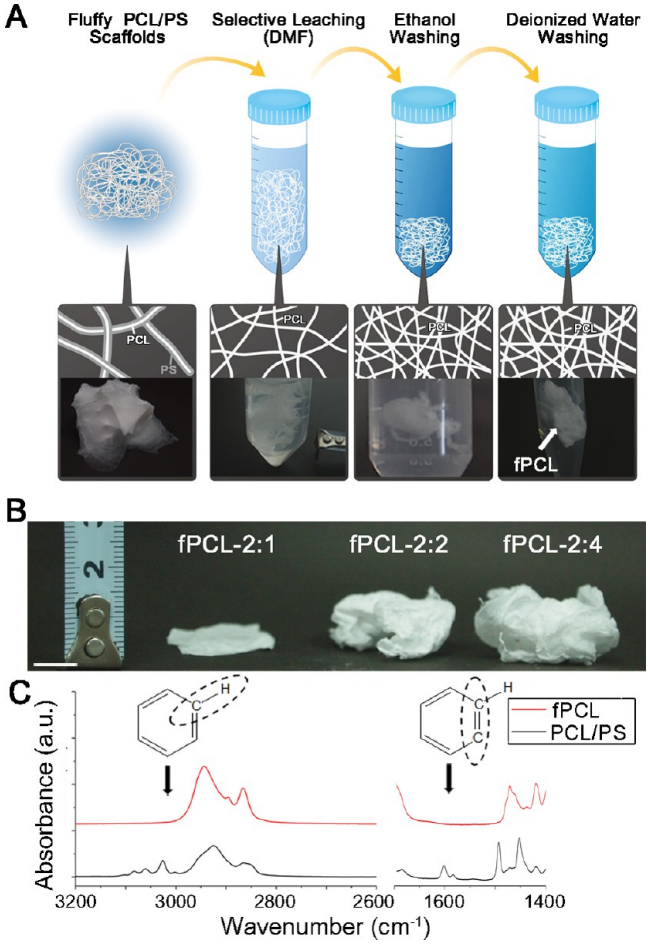

Figure 2. Fabrication of electrospun PCL–clay fibrous scaffolds (fPCLs) after the "selective" leaching process. (A) Schematic illustration of the selective leaching step followed by washing to remove the PS shell layers. (B) Digital photographs of fibrous PCL–clay scaffolds (fPCLs) after the leaching step. The scale bar represents 1 cm. (C) FT-IR analysis to confirm the removal of PS layers after the leaching step. The black arrows indicate the characteristic peak corresponding to the C–H bond and C=C bond in the PS aromatic ring.

within a prechilled DMF solution, as the solubilities of PS and PCL in DMF were clearly distinct at −20 °C (Figure S4, Supporting Information). The solubility of each material at different temperatures (−20, −10, 0, 10, and 20 °C) was determined by measuring thickness changes of PCL or PS spin-coated films, which were immersed in DMF for 1 h. As a result, PS films were completely dissolved in DMF regardless of temperatures. However, approximately 20% reduction in thickness of PCL films compared to the initial thickness was observed when the PCL films were immersed in DMF prechilled at −20 °C, confirming the distinct solubility differences between PCL and PS in DMF at −20 °C (Figure S4, Supporting Information). To completely remove the PS, the PS leaching step was conducted five times. The nanofiber mat was removed from the DMF solution and washed in ethanol at room temperature. Finally, the ethanol in the fiber mat was washed with a stream of deionized water. As shown in Figure 2B, the PCL core remained intact during the procedure, and the fluffy structures were maintained. Figure 2B shows the fluffy PCL nanofibers (fPCL-2:1, fPCL-2:2, fPCL-2:4) obtained from the PCL/PS-2:1, PCL/PS-2:2, and PCL/PS-2:4 nanofibers, respectively. To enable easy removal of the PS layer, PS was not electrospun into the core layer in this study. As controls, sheet-like PCL fibers (sPCL) or fluffy PS fibers (fPS) were fabricated by modulating the feed rates of either the PS layer or the PCL layer to zero. Removal of the PS sheath was confirmed by fast Fourier-transform infrared spectroscopy (FT-IR) analysis (Figure 2C). The characteristic peaks (1600 cm^{-1}, 3048 cm^{-1}) corresponding to the C=C and C–H bonds in the phenyl ring of PS disappeared completely after the leaching-and-rinsing process for the PCL/PS-2:2 nanofibers.

Harsh treatment such as five cycles of DMF leaching with vigorous agitation and subsequent washes with ethanol/deionized water did not cause substantial rupture or deformation of the fibrous PCL structures (i.e., fPCL-2:1, fPCL-2:2, and fPCL-2:4) (Figure 3A). The fPCL-2:1 scaffolds, which were formulated at a PS feed rate of 1 mL h^{-1} and a PCL feed rate of 2 mL h^{-1} and then subjected to the leaching process, exhibited rough fiber surfaces, while the surfaces of fPCL-2:2 and fPCL-2:4 were smooth after leaching. Vague core–shell interfaces observed in the PCL/PS-2:1 composites (Figure 1D) were subsequently leached to form fPCL-2:1 and could lead to the rough surfaces of the fPCL-2:1 scaffolds, possibly indicating that the surface morphologies of the PCL–clay scaffolds could also be related to the feed rate ratio.

In addition to the surface morphologies, the diameters of the PCL fibers were significantly affected by the PS feed rates (Figure 3B). The average diameters of the sheet-like PCL fibers (sPCL) and the fluffy PS fibers (fPS) were 0.67 ± 0.21 and 2.51 ± 0.43 μm, respectively. Before the leaching step, the average diameters of the fluffy PCL/PS scaffolds increased along with the feed rates of the PS solution. However, faster feed rates of the PS solution led to smaller diameter fPCLs after the leaching step. Consequently, fPCL-2:1, fPCL-2:2, and fPCL-2:4 scaffolds possessed diameters of 1.44 ± 0.26, 1.09 ± 0.24, and 0.81 ± 0.20 μm, respectively. The larger quantity of PS fibers deposited when the feed rate of the PS solution is greater than that of the PCL solution might increase the proportion of the electrospun fibers made up of PS, possibly increasing the volume of fluffy fibers before leaching and resulting in thinner fPCL fibers after leaching.

Interestingly, the fluffy PCL nanofiber mats exhibited an enhanced toughness or viscoelasticity, similar to rubber clay. Figure 3C displays stress–strain curves of the PCL/PS-2:2 core–sheath mat, the fluffy PCL mats (fPCLs), the sheet-type PCL (sPCL), and the PS (fPS) mats. The thickness of the sheet-type mats was 0.027 cm, and the lateral length and width were 4 and 0.5 cm. The dimension of the fluffy mats for analyzing stress–strain behaviors was approximately 4 × 0.5 × 0.07 cm. Both ends of the fluffy mats were tightly clamped for the stretching test. Young's modulus of the fPS mat and that of the core–sheath nanofiber mat were similar at 0.068 and 0.443 MPa. These mats were mechanically vulnerable at small strains and tore apart at a strain of approximately 120%. The modulus of the sPCL mat was 2.77 MPa; this sample showed elastic deformation up to a strain of approximately 50% and plastic deformation up to strains of approximately 350%. The moduli of the fluffy PCL mats (fPCLs) were lower than that of the sPCL mat, but plastic deformation occurred for strains of up to 1450% for fPCL-2:1 and 2100% for fPCL-2:2. The immersion of PCL fibers in DMF during the selective leaching step might slightly loosen PCL polymer chains in the fibers and affect the crystalline structure to make the crystalline domains imperfect, presumably increasing the flexibility of the fibrous fPCL

dx.doi.org/10.1021/am404627r | ACS Appl. Mater. Interfaces 2014, 6, 1082–1091

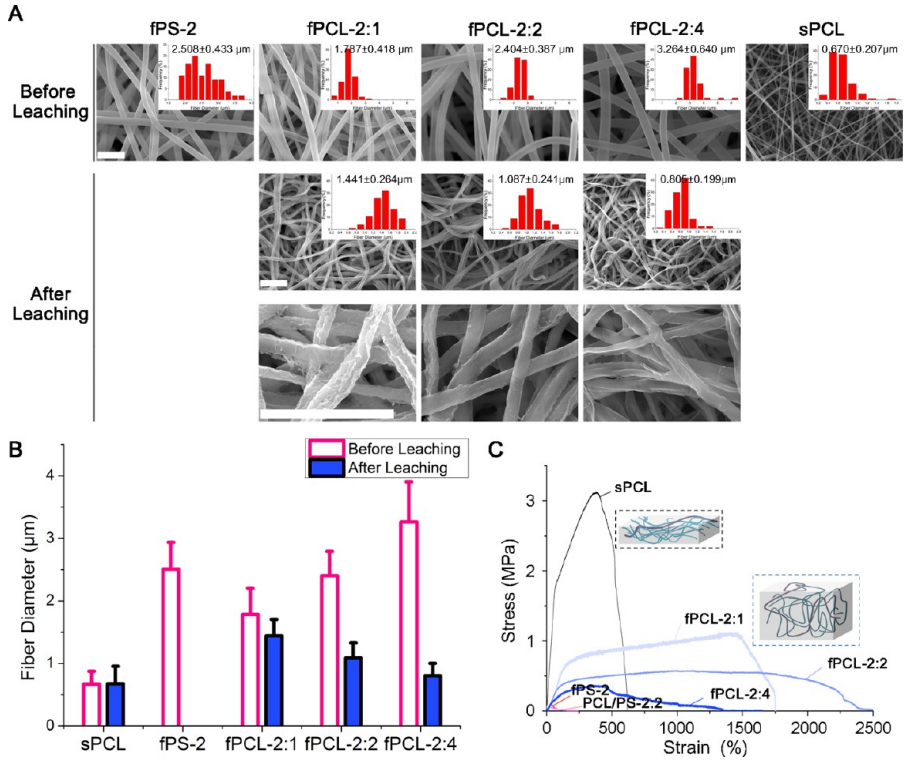

Figure 3. Characterization of fPCL–clay fibrous scaffolds. (A) Fibrous morphologies imaged using FE-SEM. Histograms indicating the distribution of fiber diameters are provided in each FE-SEM image. The scale bar represents 10 μm. (B) Average fiber diameters measured before and after the leaching step. (C) The stress–strain curves of sPCL, fPS, PCL/PS and fPCLs.

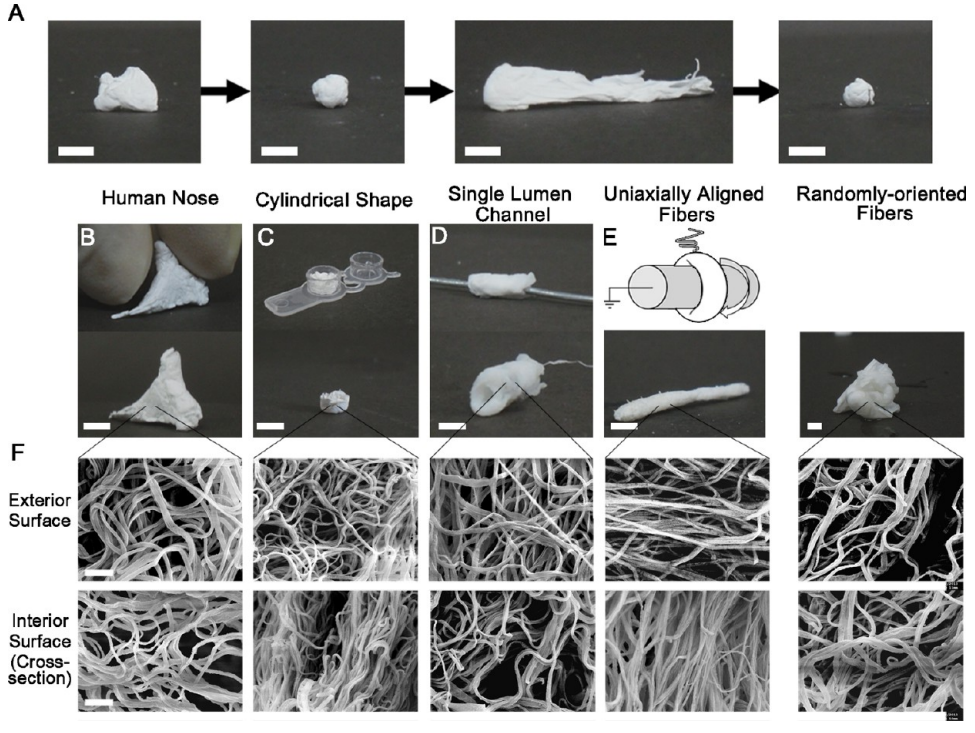

Figure 4. Clay-like properties of fPCL-2:2 fibrous scaffolds. (A) Shape change of the fPCL-2:2 scaffold. The initial cotton-like scaffold was pressed into a ball, uniaxially elongated, and then pressed again into a ball. (B–E) Transformation of the fPCL-2:2 scaffold into diverse 3-D shapes: manual pressing (human nose) (B), molding in a die (cylindrical shape) (C), and rolling on a rod (single lumen channel) (D). The fPCL-2:2 scaffold could be aligned in a uniaxial manner by the rotating mandrel (E). Fibrous microstructures of PCL–clay scaffolds were imaged using FE-SEM. FE-SEM images of the exterior surfaces (top) and the interior of each scaffold formed using fPCL-2:2 fibers. Scale bars in photographs and SEM images represent 5 mm and 10 μm, respectively.

dx.doi.org/10.1021/am404627r | ACS Appl. Mater. Interfaces 2014, 6, 1082–1091

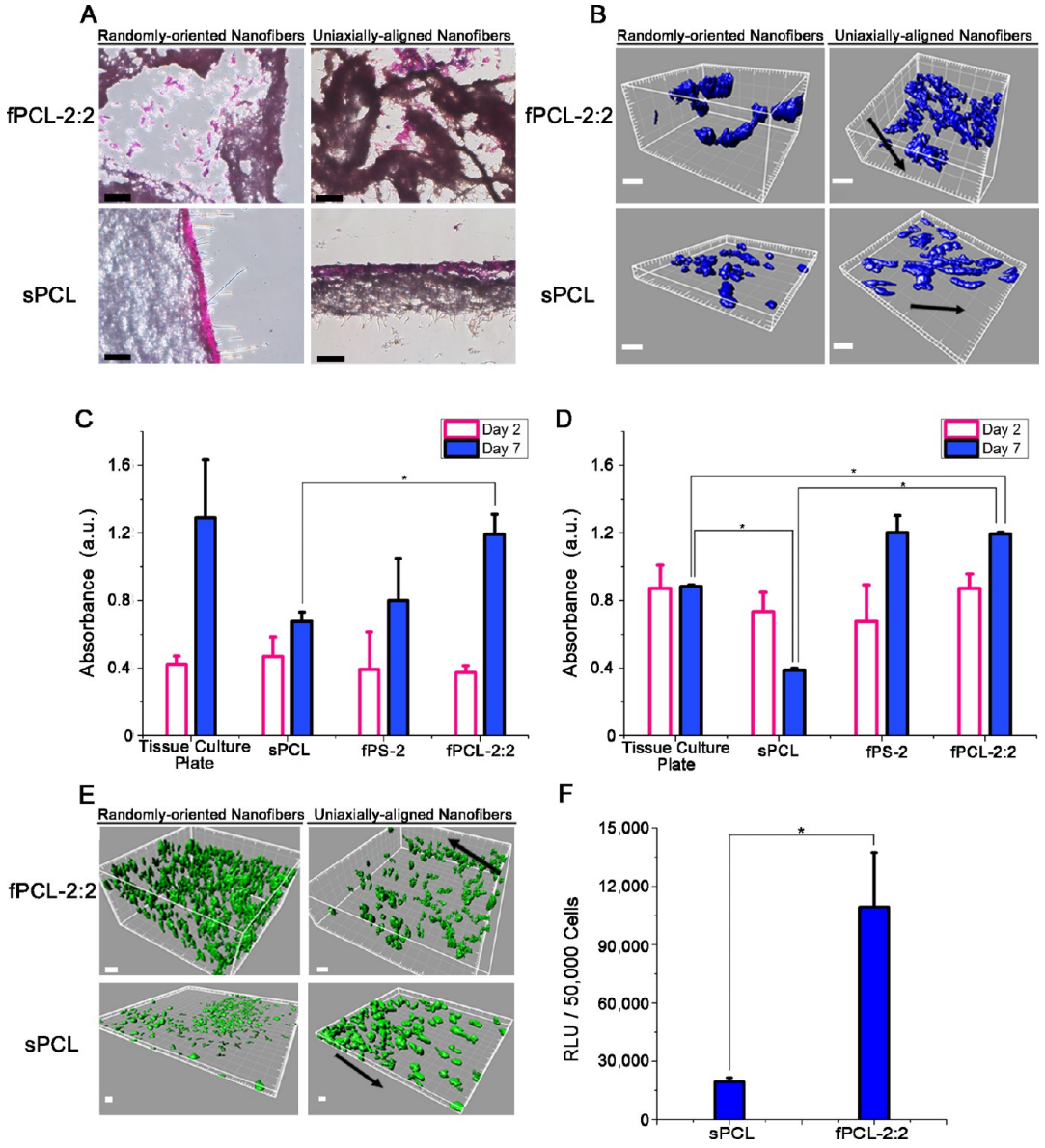

Figure 5. In vitro performance of the rubber clay-like fPCL-2:2 scaffolds. (A) Histological analysis of in vitro infiltration of the NIH3T3 cells. The cells at 4 days postculture were stained by hematoxylin and eosin for optical observation. The scale bar indicates 100 μm. (B) Confocal laser scanning microscopy (CLSM) images demonstrating the live NIH3T3 cells (stained with FDA) within the fluffy fPCL-2:2 scaffolds (top) and sPCL scaffolds (bottom) constructed by randomly oriented nanofibers and uniaxially aligned nanofibers. Cellular viabilities of NIH3T3 (C) and HEK293T (D) measured by the WST-1 assay kit. The symbol * indicates statistically significant differences ($P < 0.05$). (E) CLSM images of HEK293T cells transduced by adeno-associated viral (AAV) vectors (GFP expression vectors) preadsorbed onto the scaffolds: (top) fPCL-2:2 scaffold and (bottom) sPCL scaffolds constructed by randomly oriented nanofibers and uniaxially aligned nanofibers. The scale bars in (B) and (E) indicate 20 μm. (F) Luciferase gene expression of HEK293T cells by AAV vectors (luciferase expression vectors) preadsorbed onto the scaffolds. Relative light units (RLU) were measured on a luminometer, with levels normalized to the initial cell seeding numbers. The symbol * indicates significant differences at $p < 0.05$.

scaffolds compared to sPCL fibers. On the other hand, the differences in the mechanical properties originate from the brittleness of the nanofibers and the volumetric density of the effective networks between the nanofibers. The fPS mats and the PCL/PS core−sheath tore at low strains due to the brittle PS nanofibers and the PS sheath, whereas the ductile PCL nanofibers could yield along the strain direction.

The reduced moduli of the fluffy PCL mats are ascribed to the lower volumetric number density of the nanofibers, but they are still within the modulus range required for soft tissues in animals and humans.[33−35] The fluffy PCL nanofiber mats require only a small stress to undergo plastic deformation; this result is due to the three-dimensional conformation of the nanofibers in the fluffy mats, which differs from the two-dimensional conformation produced by the layered stacking of nanofibers in the sheet-type mats. As illustrated in the inset of Figure 3C, the contour path of each nanofiber in the fluffy mats resembles the random network configuration of polymer chains in bulk, whereas the contour path in the sheet-type mat is similar to the flattened polymer configuration of a thin polymer film. Exact tracking of the contour path should be further studied by mathematical modeling. The results show that the mechanical behavior of the fPCL-2:2 mat is similar to the viscoelastic nature of a Bingham fluid, which behaves as a rigid

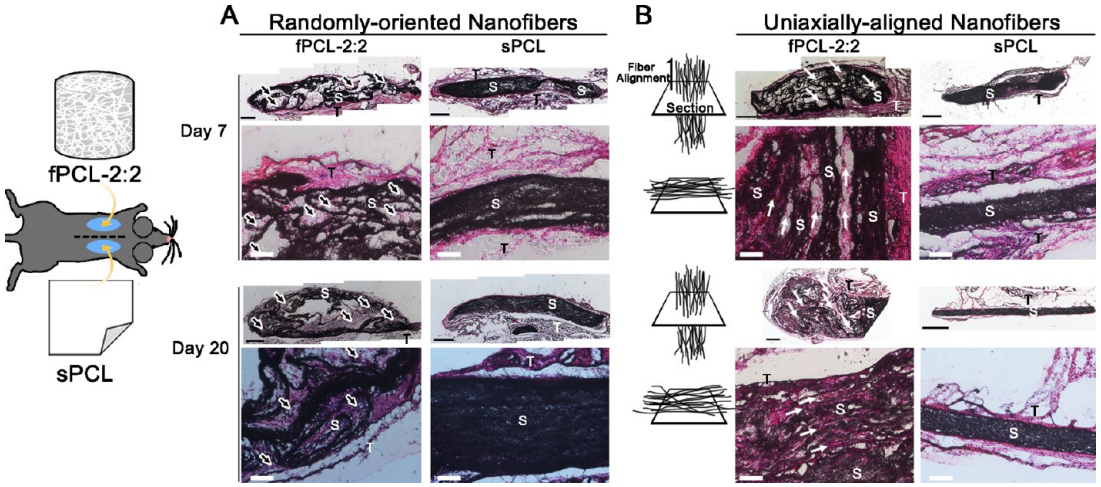

Figure 6. In vivo performance of electrospun fPCL–clay scaffolds. Scaffolds were subcutaneously implanted into mice (n = 10), and each sample was retrieved at 7 and 20 days postimplantation (randomly oriented scaffolds (A), uniaxially aligned scaffolds (B)). For images in the top row, multiple images were assembled to represent the entire scaffold. Labels indicate surrounding tissues (T) and scaffolds (S), infiltrated cells (black arrows), and infiltrated/aligned cells (white arrows). The black and white scale bars represent 500 and 100 μm, respectively.

body at low stress but flows as a viscous fluid at high stress. Such mechanical behavior is typically observed in rubber clay. Meanwhile, the fPCL-2:4 mat showed poor yielding behavior and tore at relatively low strains. These results indicate the existence of a critical number density of nanofibers in the fluffy mats for mechanically stable nanofiber concentrations.

On the basis of the stress–strain curves, the fPCL-2:2 nanofiber mat was selected for use as a scaffold. A lump of the scaffold could be elongated and then pressed into a lump again (Figure 4A), resembling the elongation and shape flexibility of rubber clay. The scaffold can be manually formed into any desired shape (e.g., a nose shape) (Figure 4B) or molded in a die to replicate a particular shape (Figure 4C). Rolling a rod against the fluffy mat generated a tubular scaffold, which could be beneficial in tissue regeneration applications requiring directional tissue growth, such as spinal cord regeneration (Figure 4D). An additional advantage of this process comes from the simple electrospinning setup. Furthermore, uniaxially aligned fluffy PCL scaffolds can be produced by collecting the core–sheath nanofibers on a rotating drum (Figure 4E). Neither direct manual contact with the fibers nor slight compression molding disrupted the fluffy structures (Figure 4F), implying that the mechanical properties of these scaffolds are sufficient to resist external forces such as cellular contractile forces or pressure occurring during the fabrication process.

To evaluate the potential versatility of the fibrous fPCL-2:2 clay scaffolds for tissue engineering applications, NIH3T3 fibroblast cells were seeded within the fPCL-2:2 scaffolds (randomly oriented and uniaxially aligned scaffolds), and cellular infiltration, distribution, and viability were examined. Staining with hematoxylin and eosin revealed well-distributed cells within both the randomly oriented and uniaxially aligned fPCL-2:2 scaffolds, whereas cells seeded onto the sheet-like sPCL fibers were primarily present on the scaffold surface (Figure 5A). Approximately 4-fold increases in pore volumes of the fluffy fPCL-2:2 scaffolds (18.082 ± 8.095 cm^3/g) compared to the sheet-like sPCL fibers (4.231 ± 0.446 cm^3/g) might result in improved cellular infiltration within the fPCL-2:2 scaffold interior (Figure S5, Supporting Information). Additionally, 3D confocal laser scanning microscope (CLSM) images illustrated that structural differences could potentially alter cellular morphologies, which may be highly critical for the induction of the functional recovery of damaged or injured tissues.[36] While cells expanded within the fPCL-2:2 randomly oriented or uniaxially aligned scaffolds likely proliferate in a three-dimensional manner, cells seeded on the surface of the sPCL scaffolds are limited to two-dimensional proliferation (Figure 5B). Cells seeded within the aligned fPCL-2:2 scaffolds were also homogeneously distributed throughout the inner space of the scaffolds and grew three-dimensionally with uniaxial patterns along the fiber alignment direction (Figure 5B). The three-dimensional environment can strongly influence the alterations in cellular morphologies, thus affecting various biological processes, including cell adhesion, proliferation, migration, and differentiation.[37] Furthermore, the natural and most favorable state of cellular expansion for inducing tissue morphogenesis may be three-dimensional cell spreading because maintaining cellular phenotypic morphology and intrinsic behavior can be highly critical to achieving proper tissue regeneration.[38]

Importantly, the three-dimensional fibrous fPCL-2:2 scaffolds provided a favorable cellular microenvironment, promoting better cell viability and proliferation compared with the two-dimensional sPCL fibers (Figures 5C and 5D). The cellular viabilities (NIH3T3 and HEK293T) within all scaffolds at 2 days postculture were similar to the viability on tissue culture plates. At 7 days postculture, cellular viabilities on the sheet-like sPCL fibers were substantially lower than that on tissue culture plates. However, cellular viabilities within the fluffy fPCL-2:2 scaffolds at 7 days postculture were either comparable (NIH3T3) or significantly improved compared to those on tissue culture plates. The increased space for cell adhesion and proliferation in the fPCL-2:2 clay scaffolds compared to the sheet-like sPCL fibers might lead to a more favorable environment for cell expansion.[19,39] Additionally, while GFP-expressing HEK293T cells transduced by AAV vectors preadsorbed onto the scaffolds were primarily observed on the exterior surfaces of the sPCL scaffolds, the transduced cells were present throughout the entire randomly oriented and uniaxially aligned fPCL-2:2 scaffold (Figure 5E). Furthermore, luciferase expression of HEK293T cells transduced by AAV vectors on the fPCL-2:2 scaffold was approximately 5-fold

enhanced compared to that on the sPCL fibers (Figure 5F), indicating the potential of these clay−fibrous scaffolds to be used for inductive tissue engineering applications.

To further investigate the in vivo performance of the electrospun clay scaffolds, both randomly oriented and aligned PCL scaffolds formed by fPCL−clay fibers and sPCL matrices were subcutaneously implanted into mice and retrieved at 7 days and 20 days postimplantation (Figure 6). Both the dimensions and the three-dimensional structures of scaffolds formulated with fPCL-2:2 clays at each time point were maintained compared with those of the initial construct, indicating that the fPCL electrospun-clay scaffolds had sufficient mechanical integrity to resist the compressive or contractile forces experienced within the in vivo environment. Importantly, at each time point, cellular infiltration was observed within the pore structures of the fPCL−clay scaffolds throughout the scaffold interior (Figure 6A and 6B), implying that the pores were interconnected. In contrast, upon transplanting sPCL scaffolds, the majority of cells was located adjacent to the exterior of the fibrous sPCL scaffolds, consistent with one of the current challenges in scaffolds fabricated by conventional electrospinning.[40] Additionally, as with the in vitro system, cellular alignment was observed along the direction of the fibrous patterns within the uniaxially aligned fPCL−clay scaffold (Figure 6B), demonstrating the significant potential of this technology to be used in directional tissue growth applications such as spinal cord regeneration.

4. CONCLUSIONS

In conclusion, three-dimensional, electrospun PCL scaffolds with "clay"-like properties have been developed by coaxially electrospinning polystyrene (in the outer layer) and poly(ϵ-caprolactone) (in the inner layer) followed by selectively leaching the polystyrene. The resulting process generated highly fluffy PS−PCL composite structures within 30 min, which represents a significant reduction in processing time compared with conventional electrospinning. The leaching process used to remove the PS shell layer yielded highly flexible PCL−clay fibrous scaffolds. Due to the clay-like properties of PCL scaffolds, the scaffolds could be formed into any desired shape without compromising the structural integrity. Importantly, cells cultured within the clay-like PCL fibrous scaffolds both in vitro and in vivo infiltrated homogeneously throughout the entire scaffolds and maintained their phenotypic morphologies and viabilities, all of which can be regarded as substantial improvements compared with conventional electrospinning. Future work should investigate combinatorial approaches including additional factors (e.g., genes or tissue inductive factors) with electrospun-clay scaffolds to induce the regeneration of specific tissues. This facile procedure enables the rapid fabrication of three-dimensional, clay-like electrospun scaffolds, and the highly favorable ECM-like cellular environment of the resulting clay-like scaffolds will extend the applicability of electrospun scaffolds to a wide variety of tissue engineering applications.

■ ASSOCIATED CONTENT

Supporting Information

Supplementary figures describing additional characteristic properties of the clay-like PCL scaffolds: Weight of the as-spun PS nanofiber mats according to the flow rate of the PS solution and the weight of the same mats after complete drying in vacuum (Figure S1). Digital photographs of the fluffy nanofiber mats obtained from the coaxial electrospinning (PCL:PS = 2:4, v/v) and a mixture solution of PCL and PS at a mixing ratio of 2:4 (Figure S2). Digital photographs of PCL/PS-2:2, PCL/PS-2:4, and PCL/PS-2:6 (Figure S3). Solubility comparisons between PCL and PS in DMF at different temperatures (Figure S4). Specific pore volume of the clay-like PCL scaffolds (Figure S5). This material is available free of charge via the Internet at http://pubs.acs.org.

■ AUTHOR INFORMATION

Corresponding Authors

*E-mail: j-jang@yonsei.ac.kr (J.H.J.).
*E-mail: ujeong@yonsei.ac.kr (U.J.).

Author Contributions

§S.L. and S.C. contributed equally. The manuscript was written through contributions of all authors. All authors have given approval to the final version of the manuscript.

Notes

The authors declare no competing financial interest.

■ ACKNOWLEDGMENTS

This work was supported by a National Research Foundation (NRF) grant funded by the Korean Government (MSIP) through the Active Polymer Center Pattern Integration (No. 2007-0056091) and Basic Science Research Program (2012R1A1A1003397) funded by the Ministry of Science, ICT & Future Planning (MSIP).

■ REFERENCES

(1) Pathi, S. P.; Lin, D. D.; Dorvee, J. R.; Estroff, L. A.; Fischbach, C. *Biomaterials* **2011**, *32*, 5112−5122.
(2) Thomas, A. M.; Kubilius, M. B.; Holland, S. J.; Seidlits, S. K.; Boehler, R. M.; Anderson, A. J.; Cummings, B. J.; Shea, L. D. *Biomaterials* **2013**, *34*, 2213−2220.
(3) Neves, S. C.; Moreira Teixeira, L. S.; Moroni, L.; Reis, R. L.; Van Blitterswijk, C. A.; Alves, N. M.; Karperien, M.; Mano, J. F. *Biomaterials* **2011**, *32*, 1068−1079.
(4) Mawad, D.; Stewart, E.; Officer, D. L.; Romeo, T.; Wagner, P.; Wagner, K.; Wallace, G. G. *Adv. Funct. Mater.* **2012**, *22*, 2692−2699.
(5) Wu, E. C.; Zhang, S.; Hauser, C. A. E. *Adv. Funct. Mater.* **2012**, *22*, 456−468.
(6) Sill, T. J.; von Recum, H. A. *Biomaterials* **2008**, *29*, 1989−2006.
(7) Liao, I. C.; Chen, S.; Liu, J. B.; Leong, K. W. *J. Controlled Release* **2009**, *139*, 48−55.
(8) Kim, B. J.; Choi, Y. S.; Cha, H. J. *Angew. Chem., Int. Ed.* **2012**, *51*, 675−678.
(9) Hansen, N. S.; Cho, D.; Joo, Y. L. *Small* **2012**, *8*, 1510−1514.
(10) Ganesh, V. A.; Dinachali, S. S.; Raut, H. K.; Walsh, T. M.; Nair, A. S.; Ramakrishna, S. *RSC Adv.* **2013**, *3*, 3819−3824.
(11) Kim, T. G.; Shin, H.; Lim, D. W. *Adv. Funct. Mater.* **2012**, *22*, 2446−2468.
(12) Liang, D.; Hsiao, B. S.; Chu, B. *Adv. Drug Delivery Rev.* **2007**, *59*, 1392−1412.
(13) Zhang, H.; Jia, X.; Han, F.; Zhao, J.; Zhao, Y.; Fan, Y.; Yuan, X. *Biomaterials* **2013**, *34*, 2202−2212.
(14) Yang, W.; Yang, F.; Wang, Y.; Both, S. K.; Jansen, J. A. *Acta Biomater.* **2013**, *9*, 4505−4512.
(15) Daud, M. F.; Pawar, K. C.; Claeyssens, F.; Ryan, A. J.; Haycock, J. W. *Biomaterials* **2012**, *33*, 5901−5913.
(16) Cao, H.; Liu, T.; Chew, S. Y. *Adv. Drug Delivery Rev.* **2009**, *61*, 1055−1064.
(17) Zhong, S.; Zhang, Y.; Lim, C. T. *Tissue Eng., Part B* **2012**, *18*, 77−87.
(18) Bonino, C. A.; Efimenko, K.; Jeong, S. I.; Krebs, M. D.; Alsberg, E.; Khan, S. A. *Small* **2012**, *8*, 1928−1936.

(19) Blakeney, B. A.; Tambralli, A.; Anderson, J. M.; Andukuri, A.; Lim, D. J.; Dean, D. R.; Jun, H. W. *Biomaterials* **2011**, *32*, 1583−1590.
(20) Coburn, J. M.; Gibson, M.; Monagle, S.; Patterson, Z.; Elisseeff, J. H. *Proc. Natl. Acad. Sci. U.S.A.* **2012**, *109*, 10012−10017.
(21) Ekaputra, A. K.; Prestwich, G. D.; Cool, S. M.; Hutmacher, D. W. *Biomaterials* **2011**, *32*, 8108−8117.
(22) Kim, T. G.; Chung, H. J.; Park, T. G. *Acta Biomater.* **2008**, *4*, 1611−1619.
(23) Bosworth, L. A.; Alam, N.; Wong, J. K.; Downes, S. *J. Mater. Sci.: Mater. Med.* **2013**, *24*, 1605−1614.
(24) Cheng, Q.; Lee, B. L.; Komvopoulos, K.; Li, S. *Biomacromolecules* **2013**, *14*, 1349−1360.
(25) Cai, S.; Xu, H.; Jiang, Q.; Yang, Y. *Langmuir* **2013**, *29*, 2311−2318.
(26) Sun, B.; Long, Y. Z.; Yu, F.; Li, M. M.; Zhang, H. D.; Li, W. J.; Xu, T. X. *Nanoscale* **2012**, *4*, 2134−2137.
(27) Langer, R.; Vacanti, J. P. *Science* **1993**, *260*, 920−926.
(28) Chen, G.; Ushida, T.; Tateishi, T. *Macromol. Biosci.* **2002**, *2*, 67−77.
(29) Jang, J. H.; Koerber, J. T.; Kim, J. S.; Asuri, P.; Vazin, T.; Bartel, M.; Keung, A.; Kwon, I.; Park, K. I.; Schaffer, D. V. *Mol. Ther.* **2011**, *19*, 667−675.
(30) Lee, S.; Kim, J. S.; Chu, H. S.; Kim, G. W.; Won, J. I.; Jang, J. H. *Acta Biomater.* **2011**, *7*, 3868−3876.
(31) Jang, J. H.; Rives, C. B.; Shea, L. D. *Mol. Ther.* **2005**, *12*, 475−483.
(32) Hwang, Y. K.; Jeong, U.; Cho, E. C. *Langmuir* **2008**, *24*, 2446−2451.
(33) Tunturi, A. R. *Physiol. Chem. Phys.* **1980**, *12*, 373−378.
(34) Ichihara, K.; Taguchi, T.; Shimada, Y.; Sakuramoto, I.; Kawano, S.; Kawai, S. *J. Neurotrauma* **2001**, *18*, 361−367.
(35) Agache, P. G.; Monneur, C.; Leveque, J. L.; Rigal, J. *Arch. Dermatol. Res.* **1980**, *269*, 221−232.
(36) Cukierman, E.; Pankov, R.; Stevens, D. R.; Yamada, K. M. *Science* **2001**, *294*, 1708−1712.
(37) Discher, D. E.; Janmey, P.; Wang, Y. L. *Science* **2005**, *310*, 1139−1143.
(38) Stevens, M. M.; George, J. H. *Science* **2005**, *310*, 1135−1138.
(39) Gurski, L. A.; Jha, A. K.; Zhang, C.; Jia, X.; Farach-Carson, M. C. *Biomaterials* **2009**, *30*, 6076−6085.
(40) Ekaputra, A. K.; Prestwich, G. D.; Cool, S. M.; Hutmacher, D. W. *Biomacromolecules* **2008**, *9*, 2097−2103.